

## Review Article

# Magnetization transfer in MRI: a review

R. M. Henkelman<sup>1,2\*</sup>, G. J. Stanisz<sup>1</sup> and S. J. Graham<sup>1</sup>

<sup>1</sup>Department of Medical Biophysics University of Toronto, Toronto, Canada

<sup>2</sup>Department of Medical Imaging, University of Toronto, Toronto, Canada

Received 18 February 2000; revised 13 October 2000; accepted 20 October 2000

**ABSTRACT:** This review describes magnetization transfer (MT) contrast in magnetic resonance imaging. A qualitative description of how MT works is provided along with experimental evidence that leads to a quantitative model for MT in tissues. The implementation of MT saturation in imaging sequences and the interpretation of the MT-induced signal change in terms of exchange processes and direct effects are presented. Finally, highlights of clinical uses of MT are outlined and future directions for investigation proposed. Copyright © 2001 John Wiley & Sons, Ltd.

**KEYWORDS:** magnetization transfer; MRI

## INTRODUCTION

Magnetization transfer (MT) in a magnetic resonance imaging (MRI) context was first discovered accidentally by Dr Bob Balaban *et al.* (Bob Balaban, private communication).<sup>1</sup> These investigators were attempting to perform a spin transfer experiment by selective saturation of urea looking for small signal suppression in water. Instead, they found a significant loss of image intensity from the proton signal in tissue, which did not depend on the specific offset frequency of the irradiation. This generalized signal suppression, now known as MT, has become accepted as an additional way to generate unique contrast in MRI that can be used to advantage in a variety of clinical applications.<sup>2,3</sup> The detailed underlying biophysics of MT is quantitatively understood, enabling MT to be optimally exploited in MRI.

## HOW MT WORKS

Proton MRI detects signal only from mobile protons

\*Correspondence to: R. M. Henkelman, Imaging and Bioengineering Research, Sunnybrook and Women's College Health Sciences Centre, 2075 Bayview Avenue, Toronto, Ontario, Canada M4N 3M5.  
E-mail: mark.henkelman@swchsc.on.ca

**Abbreviations used:**  $B_{\text{eff}}$ , effective magnetic field; CRMG, Carr–Purcell–Meiboom–Gill; CW, continuous wave; FAIR, flow sensitive alternating inversion recovery; Gd-DTPA, gadolinium diethylenetriaminepentaacetic acid; MRA, magnetic resonance angiography; MRI, magnetic resonance imaging; MS, multiple sclerosis; MT, magnetization transfer; MTR, magnetization transfer ratio; RF, radio frequency; SAR, specific absorption rate.

which have sufficiently long  $T_2$  relaxation times (i.e. greater than 10 ms) so that spatial encoding gradients can be played out between excitation and acquisition before the signal has completely decayed. The  $T_2$  of the less mobile protons associated with macromolecules and membranes in biological tissues are too short (i.e. less than 1 ms) to be detected directly in MRI. However, coupling between the macromolecular protons and the mobile or 'liquid' protons allows the spin state of the macromolecular protons to influence the spin state of the liquid protons through exchange processes. As shown in Fig. 1, it is possible to saturate the macromolecular spins preferentially using an off-resonance radio frequency pulse. The macromolecular spins have a much broader absorption lineshape than the liquid spins, making them as much as  $10^6$  times more sensitive to an appropriately placed off-resonance irradiation. This preferential saturation of the macromolecular spins can be transferred to the liquid spins, depending on the rate of exchange between the two spin populations, and hence can be detected with MRI.

Figure 2 shows a two-pool model that is simple yet sufficient for quantitative interpretation of MT.<sup>4</sup> Pool A represents the liquid spins. The number of spins in this compartment is by convention normalized to unity ( $M_{0A} = 1$ ). Pool B represents the macromolecular spins. In tissues, the number of macromolecular spins is much less than the liquid spins and the relative fraction is given by  $M_{0B}$ . In each pool, and at any instant in time, some of the spins are in the longitudinal orientation represented by the upper unshaded portion of the compartment and some spins are saturated, represented by the lower shaded portion. The partition into longitudinal spins and

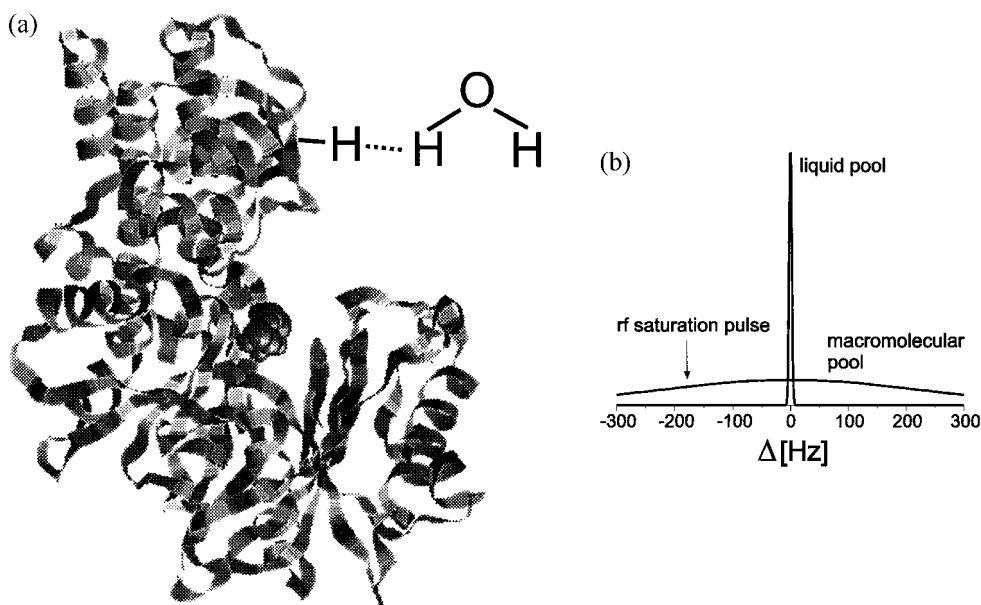


**Figure 1.** (a) Magnetization transfer exchange between macromolecular and water protons. (b) The macromolecular spins, exhibiting much broader absorption lineshape than the liquid protons, can be preferentially saturated using an off-resonance RF pulse

saturated spins depends on the prior irradiation history. When the irradiation is turned off, the time-dependent changes in the model are represented by three rate constants:  $R_A$  and  $R_B$  are the longitudinal relaxation rates of pools A and B respectively and  $R$  is the exchange rate between pools A and B. Because  $M_{0A}$  is set to 1,  $k_{AB}$  is a pseudo-first-order rate constant and the rate of transfer of spins from A to B is  $RM_{0B}$ . The rate from B to A is therefore  $R$  to conserve compartment sizes. The simple model pictured in Fig. 2 can be readily expressed by a set of coupled differential equations.<sup>4</sup>

The effect of off-resonance irradiation on this system is different for the two pools. For pool B, the protons in the macromolecules are strongly coupled to each other resulting in a homogeneously broadened absorption lineshape as is shown in Fig. 1(b). Thus, off-resonance irradiation results in progressive saturation of the ensemble of spins, with the effective saturation rate

being given by the probability of absorption at the corresponding offset frequency times the average radio frequency (RF) power at the offset frequency.<sup>5</sup>

In MT experiments, the intent is to manipulate the liquid pool indirectly by saturating the macromolecular pool. However, some direct saturation of the liquid pool is inevitable in this process and must be included in any quantitative analysis of MT effects. Because spins in the liquid pool are only weakly coupled due to motional narrowing, the effect of an off-resonance irradiation is governed by the Bloch equations. In the case of continuous wave (CW) irradiation at a single frequency off-resonance, liquid pool magnetization dynamics are most easily considered in the rf rotating reference frame, as shown in Fig. 3. In this frame, the effective field  $B_{\text{eff}}$  consists of the vector sum of the transverse  $B_1$  field and a residual longitudinal field equal to  $\Delta/\gamma$  where  $\Delta$  is the

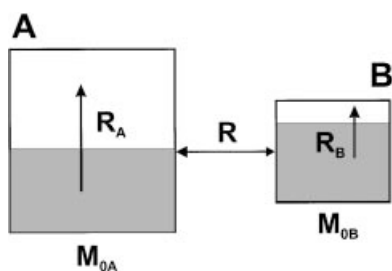


**Figure 2.** A two-pool model of magnetization transfer exchange. The shaded region in each pool represents saturated spins.  $R_A$  and  $R_B$  represent longitudinal relaxation rates in liquid and macromolecular pools respectively.  $R$  denotes magnetization transfer exchange between the pools

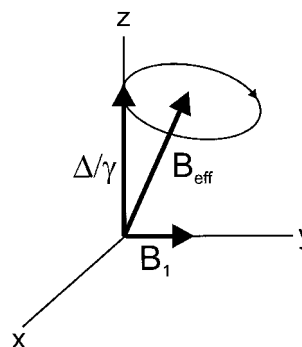


**Figure 3.** Excitation of the liquid pool magnetization with a saturation pulse of amplitude  $B_1$  and offset-frequency  $\Delta$ , results in precession about an effective field  $B_{\text{eff}}$

difference between the resonant Larmor frequency ( $\omega_0$ ) and the rotating frequency of the RF ( $\omega_{\text{RF}}$ ), as shown in Fig. 3. In MT imaging experiments, the offset frequency  $\Delta = \omega_{\text{RF}} - \omega_0$  is typically in the order of 2 kHz and the  $B_1$  field seldom exceeds a rotational frequency of 0.5 kHz due to specific absorption rate (SAR) limitations and hardware limits, ensuring that  $B_{\text{eff}}$  does not deviate from  $B_0$  by more than 15%. Nonetheless, CW off-resonance irradiation initially results in a precession of the liquid spins about the effective field and leads to transient oscillations of transverse magnetization known as Rabi oscillations which decay with a time constant of  $T_{2\rho}$ . The resultant magnetization along  $B_{\text{eff}}$  relaxes with a time constant of  $T_{1\rho}$ . To bring this picture into agreement with the simple longitudinal and saturated compartment represented in Fig. 2, it is necessary to suppress the transverse magnetization by spoiler gradients or by phase cycling. This is usually not an issue in MT imaging experiments because saturation pulses (see below) are sufficiently smooth that they are adiabatic or they are repeated sufficiently frequently that the transverse components are incoherently dephased. Irrespective of these technical issues, off-resonance irradiation inevitably produces some saturation of the longitudinal magnetization in the liquid pool.

Off-resonance irradiation in MRI can be applied in a CW mode or in a pulsed mode.<sup>6</sup> CW experiments are best for characterizing the mechanisms of the MT process because they provide the cleanest separation between the amount of saturation in the two pools. For practical imaging experiments, however, repetitive pulsed off-resonance irradiation of shorter duration is necessary to allow time for the interleaved imaging experiment, to keep the SAR within reasonable limits, and because imaging RF transmitters are designed for pulsed RF and not CW operation. Off-resonance RF pulses are usually delivered with an amplitude modulation that varies smoothly in time, such as a Gaussian envelope. The exact shape is not important provided that the Fourier transform of the off-resonance pulse does not have any amplitude in the vicinity of the Larmor frequency of the liquid pool. Alternatively, on resonance composite pulses (e.g.  $1\bar{2}\bar{2}\bar{1}$ ) can be used that saturate the macromolecular pool but flip liquid pool magnetization back to its longitudinal orientation.<sup>7</sup> Although this is an interesting concept, these pulses can produce a large amount of direct saturation of the liquid spins, depending on their  $T_2$  value, which masks the intended MT effect.<sup>8</sup> Finally, it should be noted that any off-resonance RF pulses in an imaging sequence saturate the macromolecular pool to some degree. Thus, unintended MT effects are observed in multi slice imaging when many slice selection refocusing pulses are used particularly in fast spin echo or turbo spin echo imaging<sup>9–11</sup> and in perfusion imaging with FAIR.<sup>12</sup>

The most important process in MT is the exchange between the macromolecular pool and the liquid pool. It

is this exchange that transfers macromolecular saturation to the liquid pool, resulting in decreased longitudinal magnetization being available for imaging. This spin exchange can occur via dipolar coupling or via direct chemical exchange. The model and the algebra cannot distinguish these two options, nor can the MT experiment. Experiments using isotopically substituted protons showed in a few model systems that the exchange was not chemical.<sup>13</sup> Other experiments in tissue and tissue models have shown a significant pH effect, suggesting chemical exchange, but the pH effect is too small and too broad for the whole MT exchange to be chemical.<sup>14,15</sup> Whether the exchange is dipolar or chemical, the nature of the interaction sites has yet to be determined. Are there only a few ‘docking’ sites per macromolecule that facilitate very effective exchange, or are there many possible locations for exchange that are less efficient? What are the chemical characteristics of these interaction sites? Is there any possibility of increasing the specificity of MT from a knowledge of the interaction chemistry? These are all questions related to the molecular basis of MT that require further investigation.

## EXPERIMENTAL DEMONSTRATIONS

The theoretical understanding described above has been validated in a large number of experiments by a variety of groups in tissue models and tissues, *in vivo* and *in vitro*.<sup>16–18</sup> Agreement between calculations and measured data to within 1–3% has allowed quantitative parameterization of biophysical models of MT in tissues. Agar was the first model system to be studied in detail.<sup>4</sup>

Figure 4 shows representative MT measurements for an aqueous gel sample containing 4% agar by weight.

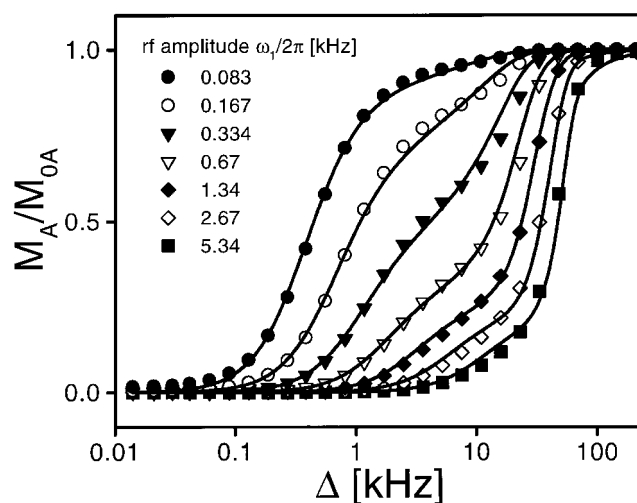


**Figure 4.** Magnetization transfer data for 4% agar. Data are plotted for seven different RF amplitudes as a function of 26 offset frequencies  $\Delta$ . Solid lines result from a two-pool model fit

The data show the fraction of longitudinal magnetization remaining after CW irradiation to a steady-state condition (7 s) as a function of the frequency offset ( $\Delta$ ) for seven different irradiation amplitudes (expressed as the nutational frequency of  $B_1$ ,  $\omega_1/2\pi$ ). The details of the experiment are given in Graham and Henkelman.<sup>6</sup> These spectra have been named *Z*-spectra by Dr Bob Bryant.<sup>19</sup> The solid lines in Fig. 4 are a fit to a two-pool model with exchange as described above. In the case of agar, the macromolecular absorption lineshape is assumed to be Gaussian—an appropriate assumption for the ‘solid-like’ agar matrix.<sup>20</sup> Over the whole data set, the average residual deviation is 1.5%. From the fitted parameters, it is learned that the effective  $T_2$  of the macromolecular spins is very short with a time constant of only 13  $\mu$ s, attesting to the immobility of the gel molecules. The fraction of macromolecular spins  $M_{0B}$  is  $0.011 \pm 0.002$ , which amounts to 60% of the stoichiometric inventory of gel protons in the sample and indicates that spin diffusion extends to most of the molecule. The fitting of the model is weakly dependent on the parameter  $R_B$ , suggesting that this parameter cannot be determined from such MT experiments.

With a quantitative model of the underlying biophysics, it is possible to ask what would happen in this MT experiment if the exchange between the two compartments did not occur. Figure 5 shows the same MT data as Fig. 4 for 4% agar at a single  $B_1$  amplitude frequency of 0.67 kHz. The upper curve shows the relative magnetization that would have been obtained if there had been no exchange between the water proton spins and those of agar. There is still saturation of the water as the offset frequency falls below 10 kHz but this

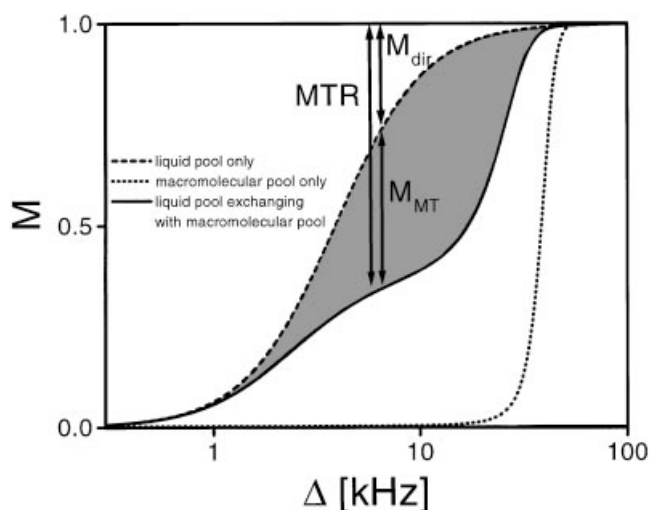


**Figure 5.** Longitudinal magnetization of the liquid and macromolecular pool for 4% agar and the amplitude of the RF saturation pulse  $B_1$  of 0.67 kHz. The shaded region between the curves illustrates the saturation due to magnetization transfer ( $M_{MT}$ ).  $M_{dir}$  indicates saturation due to the direct effect

is the direct effect of the irradiation on the water and is not due to MT. The sigmoidal shape is the irradiation profile of a Lorentzian lineshape expected for liquids plotted vs the logarithm of the frequency offset ( $\Delta$ ). The shaded region shows the amount of saturation coming from saturated agar spins exchanging with the water spins. For completeness, the dashed line shows the fraction of unsaturated agar spins without exchange if they were detected directly. The fact that they are saturated out to 35 kHz is indicative of their broad lineshape. If we consider an irradiation frequency of 8 kHz and a nutation frequency of 0.67 kHz (these would constitute an appropriate set of experimental parameters for MT imaging of agar), we can see the reduced signal  $M_{SAT}$  obtained following the saturating RF compared with the unperturbed signal  $M_0$ . It is customary in MT imaging to calculate the magnetization transfer ratio (MTR) which can be seen from Fig. 5 to consist of two contributions:  $M_{dir}$ , the direct effect contribution, and  $M_{MT}$ , the true MT contribution,

$$\begin{aligned} \text{MTR} &= \frac{M_0 - M_{SAT}}{M_0} \\ &= 1 - \left( \frac{M_{dir}}{M_0} + \frac{M_{MT}}{M_0} \right) \end{aligned} \quad (1)$$

Depending on the choice of imaging pulse sequence, this equation is slightly modified to substitute equilibrium magnetization for the effect of incomplete longitudinal recovery produced by short repetition times. Although it is important to distinguish both contributions ( $M_{dir}$  and  $M_{MT}$ ) in studies that are attempting to quantitate MT, in qualitative imaging it can be quite appropriate to have contrast generated by both MT and the direct effect. The direct effect does become more pronounced as  $T_1/T_2$  of the sample increases. Thus, some studies, which have claimed correlations of MT with either  $T_1$  or  $T_2$ , are probably influenced primarily by direct effects.

Other investigators have attempted to quantify MT images by calculating a rate constant,

$$k_{SAT} = \frac{1}{T_{ISAT}} \left[ 1 - \frac{M_{SAT}}{M_0} \right] \quad (2)$$

where  $T_{ISAT}$  is the time constant for the two pools to come to equilibrium during irradiation. As shown by Edzes and Samulski,<sup>21</sup>  $k_{SAT}$  would be the first-order rate constant for the exchange provided the macromolecular spins were kept fully saturated and provided there was no direct effect on the liquid spins. Although the algebra in eqn (2) can always be performed, the rate constant  $k_{SAT}$  has no physical meaning unless these two necessary conditions are satisfied. Originally shown by Yeung,<sup>22</sup>  $k_{SAT}$  varies from 9 to 0.7 over the offset frequency range of 1–20 kHz when calculated for the data in Fig. 5. Thus for quantitation of MT effects in imaging, MTR is a valid and useful phenomenological measure even though it

depends on tissue type and pulse sequence. In contrast,  $k_{SAT}$  purports to be a constant of the NMR dynamics, but is misleading and is bad science, because it is not a constant in tissue MT imaging.

Similar experiments to those described for agar have been performed for various biological tissues. The results are qualitatively similar and analysis with the same two-pool model can be successfully undertaken. Not surprisingly, the macromolecular absorption lineshape for tissues is not Gaussian as it is in agar, but is 'softer'. Reasonable fits can be obtained using a super-Lorentzian lineshape<sup>17</sup> as is done for liquid crystals. However, given the variety of macromolecular protons in tissue, it seems better not to use some *a priori* lineshape, but instead to let the data 'speak for itself' and to extract a parameterized absorption lineshape from the measured MT experiments.<sup>23</sup> Figure 6 shows the results of such an exercise for four different tissues. The logarithm of the absorption is plotted on the vertical axis to allow comparison of the low absorption probabilities in the tails of the distributions. The experimental lineshapes are shown only over the range of offset frequencies where they are determined to a precision of  $\pm 10\%$ . For comparison, a Gaussian distribution is shown as a dashed line and a super-Lorentzian distribution is shown as a dotted line. The super-Lorentzian is a better approximation to the experimentally derived absorption lineshapes for tissue than the Gaussian lineshape which is unacceptable. For numerical model fitting, the super-Lorentzian is more practical to use than are the experimentally derived lineshapes.

Somewhat surprisingly, the macromolecular absorption lineshape is relatively independent of tissue type even for tissues that have markedly different MTRs. The data in Fig. 6 suggest that within the complex molecular

environments in tissues, the MT exchange sites are not very different in different tissues. Given such similarity in the absorption lineshapes, why then do tissues have such different MTRs?

The amount of magnetization transfer in a tissue depends upon a competition between two processes. Longitudinal spins in the liquid pool become saturated by exchanging with macromolecular spins that have been saturated by off-resonance irradiation. The greater the exchange rate, ( $RM_{OB}$ ), the greater the MTR, but saturated spins can recover equilibrium magnetization by longitudinal relaxation mechanisms governed by  $R_A$ . The larger the  $R_A$ , the less the MTR. Thus, an appropriate indicator for the amount of MT is the ratio of the two competing rates ( $RM_{OB}/R_A$ ). Figure 7 shows the MTR for a typical MT irradiation of average amplitude 0.67 kHz and offset frequency of 8 kHz. The data point shows an MTR of 66% for white matter for this irradiation and it can be seen to be made up of 14% direct effect and 52% actual MT. If the ratio of rates that govern magnetization transfer decrease, the MTR decreases. The MTR curve is almost single valued and is shown as a single line for both the exchange decreasing with  $R_A$  fixed and  $R_A$  increasing with the exchange held constant. In either case, a drop in the ratio of rates causes a drop in the MTR. It is the ratio of rates between the two competing processes that is the primary determinate of the amount of MT for a particular irradiation experiment for different tissues. Figure 7 also explains the effect of contrast agents such as Gd-DTPA on MT imaging. Such agents increase the rate of longitudinal recovery and hence decrease the amount of MT, which must be recognized when MT imaging is performed as part of a larger examination protocol that involves prior contrast agent administration. This can be

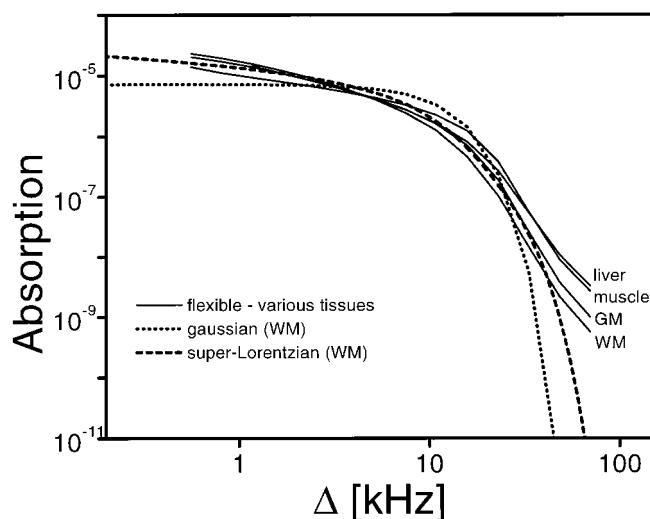


**Figure 6.** Flexible lineshapes derived from MT data for liver, skeletal muscle, gray matter (GM) and white matter (WM) in comparison to analytical Gaussian and super-Lorentzian lineshapes

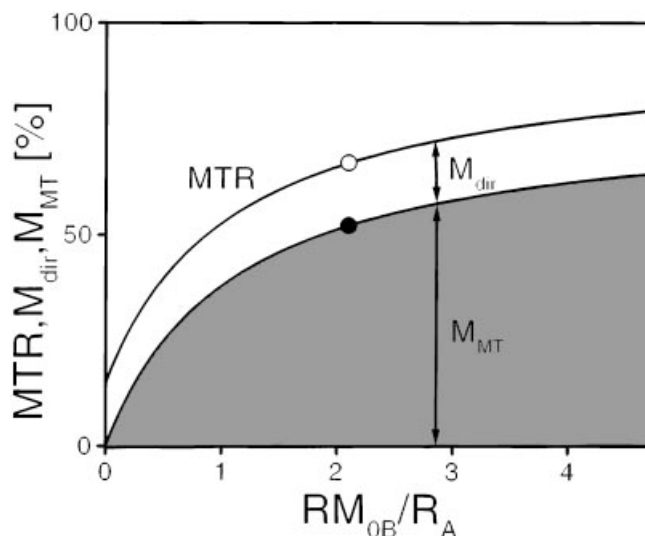


**Figure 7.** Calculated values of MTR,  $M_{dir}$ ,  $M_{MT}$  as a function of parameter  $RM_{OB}/R_A$  for  $\omega_1/2\pi = 0.67$  and  $\Delta = 8$  kHz. Experimental values of MTR and MT effect for white matter are shown as data points

used to advantage to obtain high SNR with MT contrast.<sup>24</sup> It can also be seen from Fig. 7 that the MTR for a tissue would be expected to increase as field strength increases. This is not a result of the exchange rate, which has been shown to be independent of field strength,<sup>4</sup> but is due to diminished competition from recovery of longitudinal magnetization at higher fields.

Although the discussion so far has focused on CW off-resonance irradiation for the production of magnetization transfer, the same theoretical analysis can be applied to generation of MT by pulsed irradiation.<sup>11</sup> For the effect of pulsed irradiation on the semisolid pool, the frequency content of the saturation pulse needs to be multiplied by the absorption lineshape and integrated over all frequencies.<sup>25</sup> For the liquid component, the effect of a time varying saturating pulse is best calculated from the Bloch equations. Between pulses, the two-pool system is propagated according to the model in Fig. 2. The most complete experimental verification of this model for pulsed MT in tissues is given by Sled and Pike<sup>26</sup> who have shown a similar 1–2% residual error between calculation and experiment. It can also be seen from this discussion that, holding all other experimental parameters constant, to a first approximation it is the average power of the off-resonance irradiation that determines the degree of macromolecular saturation and hence MT.

More complex models of MT have been explored. Using more than two pools is a natural extension but it has not been shown to provide a statistically better agreement to the MT data except for particularly complex tissues, such as lens of the eye.<sup>27</sup> Extending the model to include a dipolar reservoir with its own relaxation time has also been shown not to be of advantage.<sup>25,28</sup>

However, when some other NMR experiment is used to compartmentalize spins in tissue in combination with a MT experiment, it is possible to identify additional different MT compartments.<sup>29,30</sup> For example, MT combined with the Carr–Purcell–Meiboom–Gill (CPMG) sequence for measurement of  $T_2$  relaxation allows the MT properties of slowly relaxing and rapidly relaxing spins to be evaluated independently.<sup>31</sup> The analysis of such hybrid data becomes much more difficult and successful data analysis poses stringent SNR requirements that are difficult to achieve in MR imaging. Nevertheless, such multi-compartment experiments with MT have been performed on excised muscle,<sup>30</sup> nerve<sup>31</sup> and white matter.<sup>30,31,33</sup> It is quite likely that more insight about MRI of tissue water will be obtained from hybrid experiments of this type.

## APPLICATIONS IN IMAGING

Magnetization transfer is more than just a probe into the proton spin interactions within tissues. It can be used to provide additional advantageous contrast in MR images. One universally agreed upon MT application is in

magnetic resonance angiography (MRA). MRA uses specific imaging sequences to suppress the signal from static tissues while enhancing signal from blood by means of inflow or phase effects. The signal contrast between the blood and other tissue can always be enhanced by using MT (which need not affect blood) to further suppress the background tissue signal.<sup>34</sup> Better contrast between blood and tissue leads to better angiograms. The improvement produced by MT in MRA is predicted to become even greater at higher fields because of the larger MT effect. Figure 8 is kindly provided by Dr Matt Bernstein of the Mayo Clinic, Rochester, and shows superb cerebral MR angiograms acquired at 3 T with the application of MT.

The second major application of MT is characterization of white matter disease in the brain, principally multiple sclerosis (MS). MS is a diffuse, progressive disease, grossly characterized by the presence of lesions in brain white matter tissue with pathological characteristics that vary as the lesions evolve. The evolution and history of specific MS lesions is difficult to resolve with conventional  $T_1$ -weighted or  $T_2$ -weighted MRI, and some lesions are unobservable. Using MT imaging for region-of-interest analyses, however, MS lesions are more conspicuous and MTR values provide information on lesion evolution.<sup>35,36</sup> More recently, the diffuse characteristics of MS have been characterized by plotting the MTR histogram of the whole brain (Fig. 9). This process indicates that there are significant differences between the MTR ratio of the so-called ‘normal-appearing white matter’ in MS patients and the white matter of healthy individuals. Histogram-based measures of MTR show strong correlation with cognitive decline in MS patients and may provide a useful method to study the natural course of MS or to evaluate the effect of drug treatments.<sup>37</sup>

Other areas of application for MT that are less well established include breast,<sup>38</sup> knee<sup>39</sup> and cartilage.<sup>40</sup> Within cartilage, it may be possible using Gd-DTPA to separate the effect of proteoglycan degradation, from the effect of collagen disruption, which is the major contributor to MT in this tissue (Deb. Burstein, MIT, private communication).

The first application for MT was envisaged approximately 10 years ago and involved the detection of specific metabolites. Only very recently has MT from metabolites been demonstrated.<sup>41–43</sup> MT-MRS is discussed further in the article by D. Leibfritz and W. Dreher in this issue.<sup>44</sup> It is still possible that this effect will have significant application in understanding tissue metabolism in the future.

## CONCLUSIONS

Magnetization transfer is a unique contrast mechanism in MRI that has been known for the past decade. Over this



**Figure 8.** MR angiogram taken with a 3 Tesla imager with MT suppression of brain tissue of 7–16% across the image. The high Signal to Noise and MT combined to give exceptionally high quality MRAs. Image is kindly provided by Dr Matt Bernstein, Mayo Clinic, Rochester, Minnesota

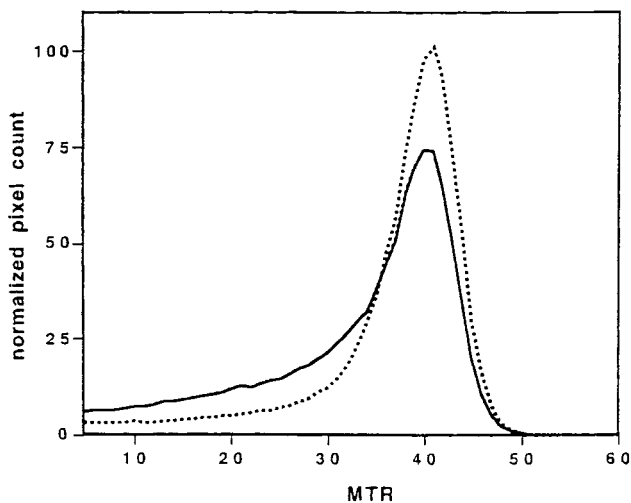


**Figure 9.** Normalized histogram of magnetization transfer ratio (MTR) for the whole brain of a healthy individual (dotted line) and a patient with multiple sclerosis (MS, solid line). The MS patient exhibits reduced peak MTR value and a larger proportion of brain pixels with low MTR values, reflecting micro- and macroscopic lesion load in the whole brain. Reproduced from Van Buchem *et al.*<sup>37</sup> with permission

period, researchers have characterized the underlying NMR physics, exchange and relaxation rates that govern MT, although detailed understanding of the chemistry and molecular interactions is still needed. Full models of MT have allowed for confident optimization of MRI pulse sequences for MT. MT has shown its value in MRA and white matter disease and holds continuing promise for use in imaging other tissues and diseases. May MT in MRI have an equally exciting second decade!

## REFERENCES

1. Wolff SD, Balaban RS. Magnetization transfer contrast (MTC) and tissue water proton relaxation in vivo. *Magn. Reson. Med.* 1989; **10**: 135–144.
2. Grossman R, Gomori JM, Ramer KN, Lexa FJ, Schnall MD. Magnetization transfer: theory and clinical applications in neuro-radiology. *RadioGraphics* 1994; **14**: 279–290.
3. Wolff SD, Balaban RS. Magnetization transfer imaging: practical aspects and clinical applications. *Radiology* 1994; **192**: 593–599.
4. Henkelman RM, Huang X, Xiang Q-S, Stanisz GJ, Swanson SD. Quantitative interpretation of magnetization transfer. *Magn. Reson. Med.* 1993; **29**: 759–766.

5. Hua J, Hurst GC. Analysis of on- and off-resonance magnetization transfer techniques. *J. Magn. Reson. Imag.* 1995; **5**: 113–120.
6. Graham SJ, Henkelman RM. Pulsed magnetization transfer imaging: evaluation of technique. *Radiology* 1999; **212**: 903–910.
7. Hu BS, Conolly SM, Wright GA, Nishimura DG, Macovski A. Pulsed saturation transfer contrast. *Magn. Reson. Med.* 1992; **26**: 231–240.
8. Graham SJ, Henkelman RM. Understanding pulsed magnetized transfer. *J. Magn. Reson. Imag.* 1997; **7**: 903–912.
9. Constable RT, Anderson AW, Zhong J, Gore JC. Factors influencing contrast in fast spin-echo MR imaging. *Magn. Reson. Med.* 1992; **10**: 497–511.
10. Dixon WT, Engels H, Castillo M, Sardashti M. Incidental magnetization transfer contrast in standard multislice imaging. *Magn. Reson. Med.* 1990; **8**: 417–422.
11. Santyr GE. Magnetization transfer effects in multislice MR imaging. *Magn. Reson. Med.* 1993; **11**: 521–532.
12. Wong EC, Buxton RB, Frank LR. Implementation of quantitative perfusion imaging techniques for functional brain mapping using pulsed arterial spin labeling. *NMR Biomed.* 1997; **10**: 237–249.
13. Ceckler TL, Balaban RS. Tritium-proton magnetization transfer as a probe of cross-relaxation in aqueous lipid bilayer suspensions. *J. Magn. Reson.* 1991; **93**: 572–588.
14. Kucharczyk W, Macdonald PM, Stanisiz GJ, Henkelman RM. Relaxivity and magnetization transfer of white matter lipids at MR imaging: Importance of cerebroside and pH<sup>1</sup>. *Radiology* 1994; **192**: 521–529.
15. Hills BP, Favret FA. A comparative multinuclear relaxation study of protein–DSMO and protein–water interaction. *J. Magn. Reson. B* 1994; **103**: 142–151.
16. Quesson B, Thiaudière E, Delalande C, Dousset V, Chateil J-F, Canioni P. Magnetization transfer imaging *in vivo* of the rat brain at 4.7 T: interpretation using a binary spin-bath model with a super-Lorentzian lineshape. *Magn. Reson. Med.* 1997; **38**: 974–980.
17. Kruiskamp MJ, de Graaf RA, van Vliet G, Nicolay K. Magnetic coupling of creatine/phosphocreatine protons in rat skeletal muscle, as studied by <sup>1</sup>H-magnetization transfer MRS. *Magn. Reson. Med.* 1999; **42**: 665–672.
18. Morrison C, Henkelman RM. A model for magnetization transfer in tissues. *Magn. Reson. Med.* 1995; **33**: 475–482. [See also Erratum. *Magn. Reson. Med.* 1996; **35**: 277.]
19. Grad J, Bryant RG. Nuclear magnetic cross-relaxation spectroscopy. *J. Magn. Reson.* 1990; **90**: 1–8.
20. Abragam A. *The Principles of Nuclear Magnetism*. Oxford University Press: London, 1961.
21. Edzes HT, Samulski ET. Cross relaxation and spin diffusion in the proton NMR of hydrated collagen. *Nature* 1977; **265**: 521–523.
22. Yeung HN. On the treatment of the transient response of a heterogeneous spin system to selective RF saturation. *Magn. Reson. Med.* 1993; **30**: 146–147.
23. Li JG, Graham SJ, Henkelman RM. A flexible magnetization transfer lineshape derived from tissue experimental data. *Magn. Reson. Med.* 1997; **37**: 866–871.
24. Jones RA, Haraldseth O, Schjøtt J, Brurok H, Jynge P, Øksendal AN, Rinck PA. Effect of Gd-DTPA-BMA on magnetization transfer: Application to rapid imaging of cardiac ischemia. *J. Magn. Reson. Imag.* 1993; **3**: 31–39.
25. Graham SJ, Henkelman RM. Quantifying the magnetization transfer produced by RF irradiation with multiple frequency components. *Proc. Int. Soc. Magn. Reson. Med.* 1996; **1**: 469.
26. Sled JG, Pike GB. Quantitative interpretation of magnetization transfer in spoiled gradient echo MRI sequences. *J. Magn. Reson.* 2000; **145**: 24–36.
27. Yeung HN, Tzou D-L, Lee SM, Huang F-Y, Hur Y. Indirect estimation of lens protein dynamics via magnetization transfer. *J. Magn. Reson. B* 1996; **113**: 167–171.
28. Morrison C, Stanisiz G, Henkelman RM. Modeling magnetization transfer for biological-like systems using a semi-solid pool with a super-Lorentzian lineshape and dipolar reservoir. *J. Magn. Reson. B* 1995; **108**: 103–113.
29. Yang H, Schleich T. *T*<sub>1</sub> discrimination contributions to proton magnetization transfer in heterogeneous biological systems. *Magn. Reson. Med.* 1994; **32**: 16–22.
30. Harrison R, Bronskill MJ, Henkelman RM. Magnetization transfer and *T*<sub>2</sub> relaxation components in tissue. *Magn. Reson. Med.* 1995; **33**: 490–496.
31. Stanisiz GJ, Kecojevic A, Bronskill MJ, Henkelman RM. Characterizing white matter with magnetization transfer and *T*<sub>2</sub>. *Magn. Reson. Med.* 1999; **42**: 1128–1136.
32. Does MD, Beaulieu C, Allen PS, Snyder RE. Multi-component *T*<sub>1</sub> relaxation and magnetization transfer in peripheral nerve. *Magn. Reson. Med.* 1998; **16**: 1033–1041.
33. Vavasour IM, MacKay AL et al., Differential magnetization transfer effects for the short and long *T*<sub>2</sub> components in white matter. *Proc. Int. Soc. Magn. Reson. Med.* 1999; **7**: 648.
34. Parker DL, Buswell HR, Goodrich KG, Alexander AL, Keck N, Tsuruda JS. The application of magnetization transfer in MR angiography with reduced total power. *Magn. Reson. Med.* 1995; **34**: 283–286.
35. Petrella JR, Grossman RI, McGowan JC, Campbell G, Cohen JA. Multiple sclerosis lesions: Relationship between MR enhancement pattern and magnetization transfer effect. *American Journal of Neuroradiology* 1996; **17**: 1041–1049.
36. Silver NC, Lai M, Symms MR, Barker GJ, McDonald WI, Miller DH. Serial magnetization transfer evolution of new MS lesions. *Neurology* 1998; **51**: 758–764.
37. Van Buchem MA, Grossman RI, Armstrong C, Polansky M, Miki Y, Heyning FH, Boncoeur-Martel MP, Wei L, Udupa JK, Grossman M, Kolson DL, McGowan JC. Correlation of volumetric magnetization transfer imaging with clinical data in MS. *Neurology* 1998; **50**: 1609–1617.
38. Santyr GE, Kelcz F, Schneider E. Pulsed magnetization transfer contrast with MR imaging with application to breast. *J. Magn. Reson. Imag.* 1996; **1**: 203–212.
39. Wolff SD, Chesnick S, Frank JA, Lim KO, Balaban RS. Magnetization transfer contrast: MR imaging of the knee. *Radiology* 1991; **179**: 623–628.
40. Kim DK, Ceckler TL, Hascall VC, Calabro A, Balaban RS. Analysis of water–macromolecule proton magnetization transfer in articular cartilage. *Magn. Reson. Med.* 1993; **29**: 211–215.
41. Dagher AP, Aletra AH, Choyke R, Balaban RS. Detection of human kidney metabolites using saturation transfer at 1.5 Tesla. *Proc. Int. Soc. Magn. Reson. Med.* 1999; **7**: 1919.
42. Meyerhoff DJ. Proton magnetization transfer of metabolites in human brain. *Magn. Reson. Med.* 1999; **42**: 417–420.
43. Roell SA, Dreher W, Leibfritz D. Combining CW and pulsed saturation allows *in vivo* quantitation of magnetization transfer observed for total creatine by <sup>1</sup>H-NMR-spectroscopy of rat brain. *Magn. Reson. Med.* 1999; **42**: 222–227.
44. Leibfritz D, Dreher W. Magnetization Transfer MRS. *NMR Biomed.* 2001; **14**: 65–76.